Nano Research
DOI 10.1007/s12274-015-0769-z
Research Article
ISSN 1998-0124
CN 11-5974/O4

A new insight into electrochemical detection of eugenol by hierarchical sheaf-like mesoporous $NiCo_2O_4$

M.U. Anu Prathap, Chao Wei, Shengnan Sun and Zhichuan J. Xu(✉)

Nano Res., **Just Accepted Manuscript** • DOI 10.1007/s12274-015-0769-z
http://www.thenanoresearch.com on March 26, 2015

Just Accepted

TSINGHUA UNIVERSITY PRESS Springer

TABLE OF CONTENTS (TOC)

A New Insight into Electrochemical Detection of Eugenol by Hierarchical Sheaf-like Mesoporous $NiCo_2O_4$

M.U. Anu Prathap, Chao Wei, Shengnan Sun and Zhichuan J. Xu*

School of Materials Science and Engineering, Nanyang Technological University, 50 Nanyang Avenue, Singapore 639798, Singapore.

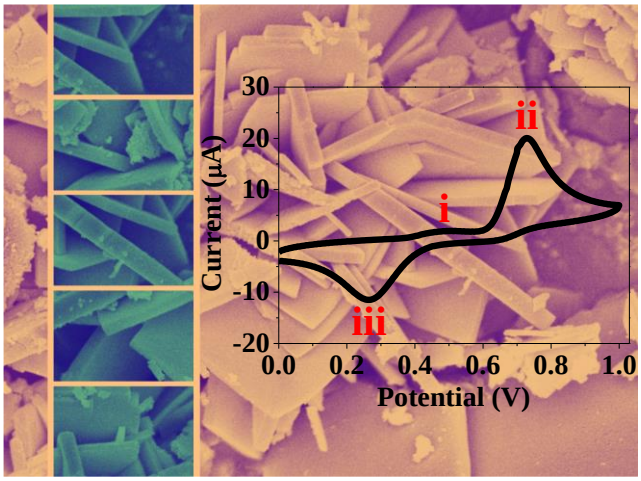

A highly sensitive and selective non-enzymatic eugenol sensor has been successfully constructed using high surface area mesoporous $NiCo_2O_4$. The sensor exhibits a low detection limit of 5.4 pM.

Nano Res
DOI (automatically inserted by the publisher)
Review Article/Research Article **Please choose one**

A New Insight into Electrochemical Detection of Eugenol by Hierarchical Sheaf-like Mesoporous $NiCo_2O_4$

M.U. Anu Prathap, Chao Wei, Shengnan Sun and Zhichuan J. Xu(✉)

School of Materials Science and Engineering, Nanyang Technological University, 50 Nanyang Avenue, Singapore 639798, Singapore.

Received: day month year / Revised: day month year / Accepted: day month year (automatically inserted by the publisher)

ABSTRACT

In this work, $NiCo_2O_4$ nanosheet with sheaf-like nanostructure morphologies was synthesized by a facile one-step hydrothermal reaction followed by annealing treatment. Impressively, the $NiCo_2O_4$ exhibit rapid detection of eugenol. The linear range of detection is from 1-500 μM, and the limit of detection is 5.4 pM. $NiCo_2O_4$ modified electrode demonstrated high sensitivity, good repeatability and reproducibility, and long-term stability (7 % decrease in response over 30 days). Based on this work, an electrochemical reaction mechanism for eugenol oxidation was proposed, and in addition, the $NiCo_2O_4$ modified electrode was successfully employed for the analysis of eugenol in medicative balm samples. The recoveries study for eugenol in medicative balm samples gave values in the range of 98.7–105.5%.

KEYWORDS

$NiCo_2O_4$ nanosheets, Eugenol determination, Electrocatalysis, Electrochemical mechanism, Real sample analysis.

1. Introduction

Medicinal aromatic plants present a number of beneficial properties to human health and well-being [1, 2]. Essential oils from these plants are anti-oxidant, digestion-stimulating, hypolipidemic, anti-inflammatory and anti-carcinogenic [1, 2]. Phenolic and polyphenolic compounds contained in essential oils are responsible for their high anti-oxidant capacity beneficial to the food industry as preservatives [3]. Eugenol (4-allyl-2-methoxyphenol), the main flavor chemical of cloves, are used extensively as additives in foods, formulations of different cosmetic or aromatherapy products and also in diverse industrial products [1-3]. It is used in the production of isoeugenol for the manufacture of vanillin which is an artificial substitute for vanilla [3]. Since it is an antioxidant it is useful in the manufacture of plastics and rubbers [1-3]. However, at higher concentration, eugenol acts as a strong oxidant causing increased generation of tissue-damaging free radicals causing inflammatory and allergic reactions, due to the formation of phenoxyl radicals and subsequently of

Address correspondence to xuzc@ntu.edu.sg

quinine intermediate [4, 5]. Additionally, it has been reported to have respiratory infection, aspiration pneumonitis, hemoptysis, and hemorrhagic pulmonary edema in individuals [1-5]. Allergy to eugenol used in dentistry is a topical issue and has been the subject of recent papers and editorial [6]. According to the Food and Agriculture Organization (FAO) and the World Health Organization (WHO) have suggested tolerable human eugenol daily dose of 2.5 mg kg^{-1} body weight [7]. Different types of chromatography techniques have been successfully applied for eugenol quantification [8, 9]. In spite of the significant advances of these methods, reported techniques are time-consuming, labor-intensive, and require relative expensive and complicated instrumentation. Compared to the existing methods, electrochemical sensing strategies have spurred intense interest in the research community due to their simplicity, low cost, and high sensitivity [10, 11]. Electrochemical sensors provide illimitable opportunities for monitoring health and making the world safer and cleaner [10, 11]. For these reasons, sensible and selective electrochemical methods are necessary for systematic investigation of eugenol. Nevertheless, the electrochemistry of eugenol has been less investigated, but they are known to be oxidized to o-benzoquinone [12].

The development of nanomaterials based sensor facilitated by recent advances is having a major impact on online environmental monitoring and food safety applications [13-16]. In recent years, $NiCo_2O_4$ nanomaterials have attracted increasing attention in material science, analytical science, and biomedical applications [17-19]. Generally, electrode materials with hierarchical porous structures exhibit many advantageous properties, which are favorable for improving the electrochemical performance [17-19]. Various synthesis techniques have been employed to prepare $NiCo_2O_4$ with different shapes and sizes [20-25]. Up to now, a variety of zero-, one-dimensional $NiCo_2O_4$ nanostructures, such as nanotubes, nanoparticles, nanorods and nanosheets, have been applied in fabricating electrochemical biosensors [26-28]. Recently, two dimensional (2D) nanosheets or nanoplates, which are made of single or a few layers, have garnered a remarkable attention as their quantum size effect brought unique physical properties [29]. However, the effective utilization of two-dimensional $NiCo_2O_4$ nanostructures in high-performance sensors is still a challenge. Therefore, the synthesis of $NiCo_2O_4$ with a rationally designed is imperative.

In this work, we have demonstrated that $NiCo_2O_4$ nanosheets can be synthesized with sheaf-like nanostructure morphologies under facile hydrothermal and thermal decomposition process. The $NiCo_2O_4$ modified electrodes are fabricated and applied to study the electrochemical behavior of eugenol. This work for the first time explores the detailed kinetics and mechanism of oxidation of eugenol in the acidic medium. Electrochemical measurements reveal high sensitivity, low detection limit for eugenol.

2. Experimental

2.1. Chemicals

All chemicals were analytical grade and used without further purification. $Ni(NO_3)_2.6H_2O$, $Co(NO_3)_2.6H_2O$, NaOH, citric acid, sucrose, glucose, tartaric acid, eugenol, dopamine, L–dopa, catechol, and urea were obtained from Sigma-Aldrich. Deionized water from Millipore Milli-Q system (Resistivity 18.2 MΩ cm) was used in the electrochemical studies.

2.2. Preparation of citrate buffer

Electrochemical experiments were performed in solutions containing x ml of 0.1 M sodium citrate dihydrate + y ml of 0.1 M anhydrous citric acid, with x and y varied conveniently to cover the 3–6.2 pH range. It was used as the supporting electrolyte.

2.3. Treatment of real sample

For real sample preparation, 1.0 g of medicative balm (from local market) was weighed and placed into a 50 mL polytetrafluoroethylene (PTFE) centrifuge

tube, and pure ethanol (10.0 mL) was added. After 15 min of sonication, the mixture was centrifuged at 4000 rpm for 5 min. The supernatant was transferred quantitatively into a 100 mL volumetric flask. The above extraction procedure was repeated 5 times. All extracts were collected, and transferred into a 100 mL volumetric flask; then, the solution was diluted to the mark with ethanol. Aliquot of this sample solution was analyzed by the voltammetric procedure.

2.4. Preparation of $NiCo_2O_4$

$NiCo_2O_4$ was prepared by following the modified method to a reported procedure which is described here in detail [18]. In a particular synthesis, 0.58 g $Ni(NO_3)_2.6H_2O$, 1.17 g $Co(NO_3)_2.6H_2O$, and 2.4 g urea were dissolved in 40 mL distilled water and stirred for about 10 minutes to obtain a transparent pink colored solution. The reaction mixture was then transferred into a Teflon-lined stainless steel autoclave, and hydrothermally treated at 433 K for 12 h. Autoclave was cooled to room temperature and the reaction mixture was filtered, washed with distilled water and ethanol, followed by drying at 353 K for 24 h. Finally, the material was calcined at 673 K for 4 h using programmable furness by maintaining the heating rate of 2 ^{o} min^{-1}.

2.5. Characterizations

The as-prepared materials were characterized with X-ray powder diffractometer (XRD; Shimadzu XRD-6000, Cu Kα radiation) at a scan rate of 1° min^{-1}. Scanning Electron Microscopy (FESEM, JSM-7600F) and transmission electron microscopy (TEM; JEOL, JEM-2100F) operated at 200 kV was used to observe the morphological features. Nitrogen adsorption measurement at 77 K was performed by Tristar-3000 surface area analyzer. Samples were out-gassed at 423 K for 4 h in the degas port of the adsorption apparatus. The specific surface area was determined by Brunauer–Emmett–Teller (BET) method using the data points of P/P_0 in the range of about 0.05–0.3. The ultraviolet-visible diffuse reflectance spectrum (UV-vis DRS) was obtained on a UV-visible spectrophotometer (Shimadzu UV-2501PC). Thermogravimetric analyses (TGA) were performed on a TGA Q500 under air atmosphere.

2.6. Electrochemical measurements

Cyclic voltammetry (CV), Linear sweep voltammetry (LSV) and chronoamperometric studies were performed by using a computer-controlled Pine Instrument. A three electrode electrochemical cell was employed with Ag/AgCl as the reference electrode (3M KCl), metal oxide mounted glassy carbon electrode (GCE) (0.196 cm^2) as the working electrode, and Pt foil as the counter electrode. Before modification of GCE, the polished electrode was ultrasonicated in ethanol and deionized water for 5 minutes, respectively. The working electrodes were prepared as follows: 10 µL aliquot of metal oxide suspension (a homogenous sonicated solution of 10 mg of $NiCo_2O_4$ and a mixture of 0.1 mL of Nafion and 0.9 mL of water) was placed onto the electrode surface; the electrode was dried in air leaving the material mounted onto the GCE surface.

3. Results and Discussion

3.1. Physico-chemical characterization

The crystallographic information of the phase changes of the as-synthesized samples were established by powder XRD. The precipitate, before calcination processing, was collected and subjected to XRD investigation. All the diffraction peaks are attributable to the nickel cobalt hydroxy carbonate (NCHC) precursor (JCPDS 29-0868) (Figure S-1 in the ESM). XRD pattern of the product obtained after calcination can be index to cubic spinel of $NiCo_2O_4$ (JCPDF card: 20-0781) with lattice constants a = b = c = 8.11 Å (Fig. 1(a)).The sharp peaks indicate that the $NiCo_2O_4$ samples are well crystallized illustrate good crystallinity of the $NiCo_2O_4$ materials, which can be attributable to the unique environment of hydrothermal reaction for crystal growth. The FESEM was employed to examine the morphologies

of the $NiCo_2O_4$ samples, and the panoramic views exhibited hierarchical sheaf-like structures consisting of nanosheets (Fig. 1(b)). TEM measurements were further carried out to analyze the nanostructures of $NiCo_2O_4$ nanosheets. It can be seen that the observed nanosheets have a thickness in the range of 90–120 nm (Fig. 1(c)). Notice that the entire surfaces of $NiCo_2O_4$ are two-dimensional nanosheets. A high-resolution TEM (HRTEM) image taken from a single nanocrystal within a $NiCo_2O_4$ nanosheet is depicted in Fig. 1(d). A lattice fringe with a *d*-spacing of 0.24 nm was calculated, corresponding to the (311) plane of spinel $NiCo_2O_4$. Fig. 1(e) schematically shows the synthesis of the $NiCo_2O_4$ nanosheet. The hydrothermal processing time, temperature, the type of mineralizing agent (urea) and its concentration resulted into NCHC nuclei. Further, these particles coalesce and undergo ripening processes. However, at a higher temperature nanosized crystals seem to grow fast enough to produce nanosheet-like form. These crystals are thermodynamically favored to split into different directions based on crystal splitting theory [30]. The investigations of the thermal behavior of NCHC coprecipitate by the thermogravimetric analysis (TGA) is shown in Fig. 2(a). There is a net weight loss of 23.1% in the temperature range between 313 K and 873 K. The observed weight loss indicates thermal decomposition of nickel cobalt hydroxyl carbonate precursor. Moreover, according to the TGA results (Fig. 2(a)), the calcination temperature of 673 K, in air, is high enough to ensure the formation of $NiCo_2O_4$ as a single phase. The relevant chemical reactions involved can be presented as eqns [31]:

$$(Co^{2+},Ni^{2+}) + CO_3^{2-} + OH^- \rightarrow (Co, Ni)_2CO_3(OH)_2 \quad (1)$$

$$Ni_2CO_3(OH)_2 + 2Co_2CO_3(OH)_2 + O_2 \rightarrow 2NiCo_2O_4 + 3CO_2 + 3H_2O \quad (2)$$

To further investigate the specific surface area and porous nature of $NiCo_2O_4$, Brunauer–Emmett–Teller (BET) gas-sorption measurements were performed. N_2 adsorption–desorption isotherms at 77 K are reported in (Fig. 2(b)), with the insets showing their corresponding Barrett–Joyner–Halenda (BJH) pore-size distribution. The $NiCo_2O_4$ shows a distinct type IV isotherm with H3 hysteresis loop in the larger range ca. 0.45–1.0 P/P_0, indicating the presence of mesopores formed by porous stacking of component nanoparticles [18]. According to the corresponding BJH plots (Fig. 2(b), inset) recorded from the nitrogen isotherms of the $NiCo_2O_4$ samples, the average pore diameter is about 3.9 nm along with a wide pore size distribution centered at ~32.6 nm, respectively, confirming that the sample contains mesoscale pores [18]. The BET specific surface area and pore volume of the sample were 83.8 m^2g^{-1} and 0.16 $cm^3\,g^{-1}$ for $NiCo_2O_4$ nanosheets.

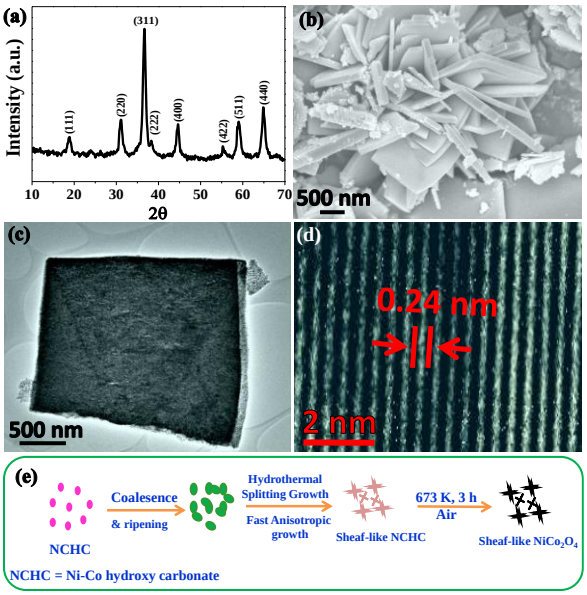

Figure 1 (a) XRD pattern of $NiCo_2O_4$, (b) SEM image of $NiCo_2O_4$, (c,d) TEM images of $NiCo_2O_4$; the inset of (d) show the SAED, and (e) Plausible formation mechanism of sheaf-like $NiCo_2O_4$.

Diffused reflectance UV–visible (DRUV–visible) investigation was used to determine the electronic structure and optical properties of $NiCo_2O_4$. It is generally known that in the spinel structure of $NiCo_2O_4$, the divalent cations Co^{2+} (half) occupy the

tetrahedral sites, whereas the trivalent Ni^{3+} and Co^{3+} cations (the other half) reside in the octahedral sites [18]. The band gap energy (E_g) can be calculated by the following equation :

$$(\alpha E_{photon})^2 = K(E_{photon} - E_g) \qquad (3)$$

Where α is the absorption coefficient, E_{photon} is the discrete photon energy; K is a constant relative to the material. The plot of $(\alpha E_{photon})^2$ vs E_{photon} based on the direct transition is shown in (Fig. 3(a), inset). The extrapolated value (the straight lines to the x axis) of E_{photon} at α = 0 gives an absorption edge energy corresponding to E_g. Using DRUV-visible, E_g of the $NiCo_2O_4$ were found to be 2.1 and 4.3 eV [18]. It is well-known that the E_g of a semiconductor increases with a decrease in grain size; this is attributed to the presence of defect sites.

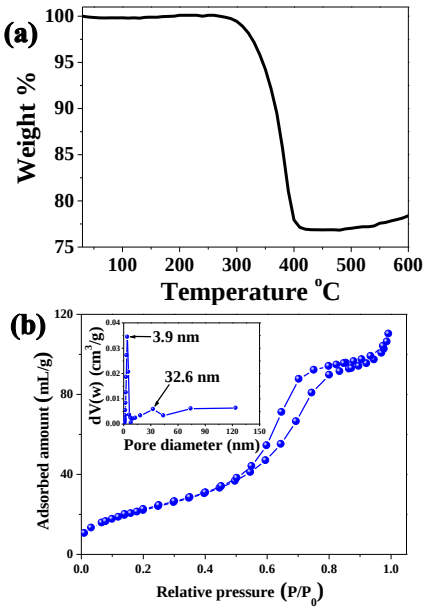

Figure 2 (a) TGA curve of nickel cobalt hydroxy carbonate precursors. (b) N_2 adsorption–desorption isotherm of $NiCo_2O_4$. Inset shows pore size distribution of $NiCo_2O_4$ sample.

3.2. Electrochemical characteristics of $NiCo_2O_4$ modified electrode

Prior to the implementation for the electrochemical detection of eugenol, the electrochemical behavior of $NiCo_2O_4$ modified electrodes was investigated using CV in 0.1 M NaOH solution. The electrochemical behavior of $NiCo_2O_4$ modified electrode was investigated using CV in 0.1M NaOH solution. $NiCo_2O_4$ modified electrode exhibits well-defined redox peaks (Fig. 3(b)) corresponding to the oxidation of Co(II) and the reduction of Ni(III). These anodic peaks can be correlated with the oxidation of Co(II) to Co(III) to Co(IV) [32, 33]. The cathodic peaks correspond to the reduction of Co(IV) to Co(III) to Co(II) and Ni(III) to Ni(II) [32, 33]. It may be noted that the redox potential of Ni(II)/Ni(III) is very close to Co(III)/Co(IV) [32, 33]. The enclosed area of CV loop of the $NiCo_2O_4$ is larger, implying its better electrochemical reactivity.

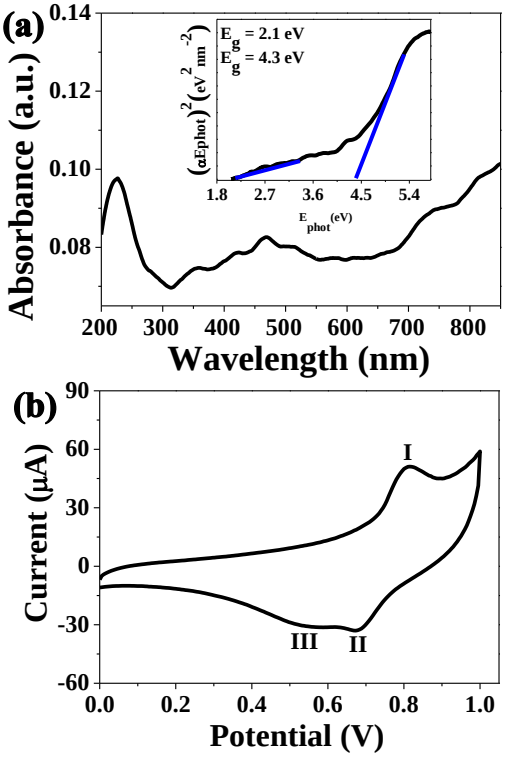

Figure 3 (a) DRUV–visible spectrum of $NiCo_2O_4$. Inset shows the plot of $(\alpha Ephoton)^2$ vs. Ephoton for $NiCo_2O_4$. (b) CV of $NiCo_2O_4$ modified electrode in 0.1 M NaOH.

3.3. Mechanistic study of eugenol at $NiCo_2O_4$ modified electrode

To verify this proposal, $NiCo_2O_4$ modified electrode was constructed to obtain the optimized analysis parameter for eugenol detection. The representative cyclic voltammograms of eugenol at $NiCo_2O_4$ modified electrode in pH 6.0 solution are shown in Fig. 4(a). A weak (i) and a well-defined (ii) oxidation peak oxidation peaks were observed at 0.48 V and 0.72 V for eugenol (Fig. 4(a)) during the sweep from 0.0 to 1 V, and reduction peak (iii) on the negative scan, which demonstrated that anodic peak (i) and cathodic peak (iii) were reversible. These one pair of peaks corresponded to oxidation/reduction of catechol [16]. Consecutive CVs of eugenol at the $NiCo_2O_4$ modified electrode in the citrate buffer pH 6.0 with a scan rate of 20 mV/s (Fig. 4(a)) showed that there was only one oxidation reaction corresponding to the formation of one electroactive product [12]. According to the literature [12, 16], we propose a reaction mechanism for electrochemical oxidation of eugenol in the acidic medium. We conduct an experiment by studying the scan rate effect to the charge transfer process of the as-formed peak to verify the proposed approach to the selective recognition of eugenol. Fig. 5(a) shows the cyclic voltammograms and the plot of peak current versus scan rate at different scan rates ranging from 20 to 600 mV/s. A good linear relationship to the peak current and square root of scan rate undoubtedly indicates a diffusion controlled process [16, 34]. The effect of applied potential on the response current of the sensor was investigated. Amperometric response at $NiCo_2O_4$ modified electrode on addition of 50 µM eugenol at different applied potentials (ranging from 0 to 0.75 V) was measured (Fig. 5(b)). In the range of 0.6 to 0.75 V, the oxidation current of eugenol increased by increasing potential. The maximum response current with a good signal/noise ratio was achieved at 0.75 V, which match with CV curves.

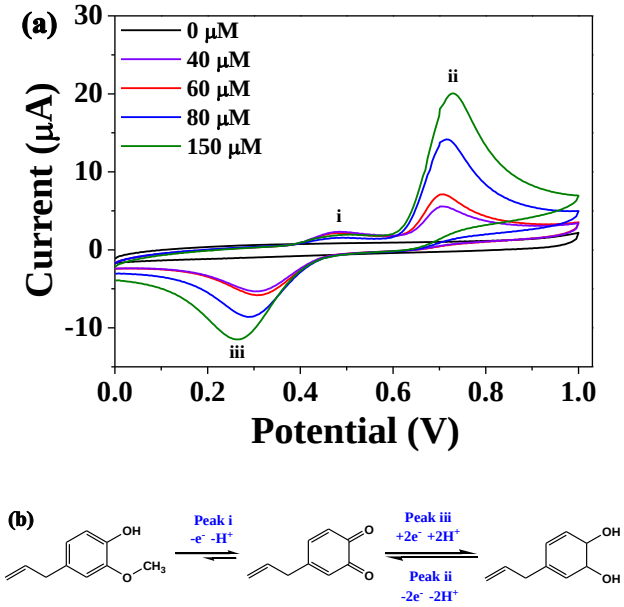

Figure 4 (a) Consecutive CVs of eugenol at $NiCo_2O_4$ modified electrode in 0.1 M citrate buffer pH 6.0 with a scan rate of 20 mV/s. (b) Electrochemical reaction mechanisms of eugenol oxidation at $NiCo_2O_4$ modified electrode.

Figure S-2 in the ESM demonstrated the influence of the pH of buffer solution on the electro-oxidation peak potential and its corresponding anodic current of eugenol at $NiCo_2O_4$ modified electrode. With the pH value of buffer solution increased from 3.0 to 6.2, the anodic potential decreased gradually. When the pH value increased from 3.0 to 6.2, the anodic peak current of eugenol increased. Nevertheless, when the pH was beyond 6.0, the peak current conversely decreased. This phenomenon was probably due to the dissociation of the phenolic moiety in eugenol to produce the corresponding anion. Therefore, considering the sensitive determination for eugenol pH 6.0 was chosen for the subsequent analytical experiments.

Under the optimized conditions, linear sweep voltammetry was used to determine eugenol. LSVs were carried out using $NiCo_2O_4$ modified electrode with increasing concentration of eugenol.

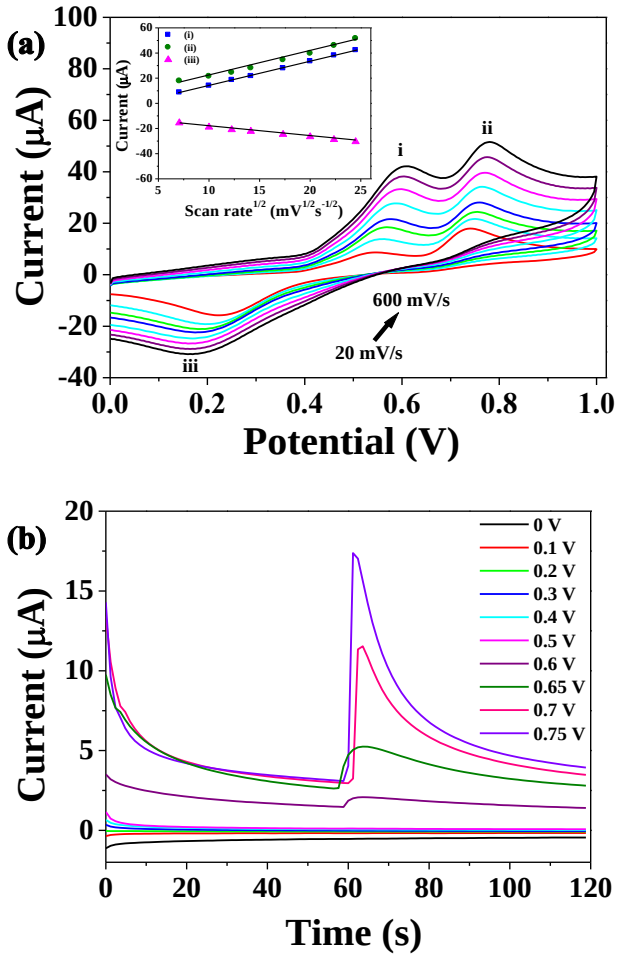

Figure 5 (a) CVs of eugenol in 0.1 M citrate buffer (pH 6.0). Scan rates from 20 to 600 mV/s. Inset: plots of peak currents versus the square root of the scan rate. (b) Effect of applied potential on the detection of eugenol in 0.1 M citrate buffer (pH 6.0) at $NiCo_2O_4$ modified electrode.

In the absence of eugenol, no peak was observed. When eugenol was added, a distinct peak for the oxidation of eugenol was appeared (Fig. 6(a)). As can be seen, the peak current (I_p) of eugenol increases with its concentration. A linear dynamic relationship in the concentration range of 1-500 μM with a calibration equation of I(μA) = 3.33 + 0.047 C (μmol L^{-1}) (R^2 = 0.9979) (Fig. 6(a), inset). The sensitivity is 0.2397 μA μM^{-1} cm^{-2}; and a lower detection limit of 5.4 pM. The limit of detection was calculated by using IUPAC (International Union of Pure and Applied Chemistry) definitions, using the standard approach of alternative (SA) [35].

$$LOD_{SA} = 3S/q \qquad (4)$$

Where S is the standard deviation of the blank signal, and q is the slope of the calibration curve. A comparison of analytical performance between the proposed method and all the previously published methods for eugenol is summarized in Table S-1 in the ESM. The detection range of this method is quite wide compared with the listed methods. Moreover, to the best of our knowledge, the detection limit of this work is among the lowest ones that have been reported so far [12, 36-41]. In this work, we found that the bare glassy carbon electrode was unqualified for the successive measurements because the oxidation peak currents of eugenol decreased continuously, it may be attributable to the sluggish electron kinetics, restricted diffusion of the analyte, and electrode fouling (Figure S-3 in the ESM) [42].

3.4. Selectivity, stability, and reproducibility of the $NiCo_2O_4$ modified electrode

The potential interferences for the detection of eugenol were studied. Under the optimized conditions, the oxidation peak current of eugenol was individually measured in the presence of different concentrations of interferents and the peak current change was then checked. No influence on the detection of 50 μM eugenol is found after the addition of 2000–fold concentration of Mg^{2+}, Na^+, Zn^{2+}, NO_3^-, K^+, Fe^{3+}, Al^{3+}, Ca^{2+}; 1500–fold concentration of Cu^{2+}; 2000–fold concentration of citric acid, sucrose, glucose, tartaric acid; 1000–fold concentration of glycine; 100–fold concentration of uric acid; 80–fold concentration of levomenthol, D-camphor, cajeput oil, peppermint oil, dopamine, L–dopa, and 20–fold concentration of ascorbic acid and catechol (peak current change <7%).

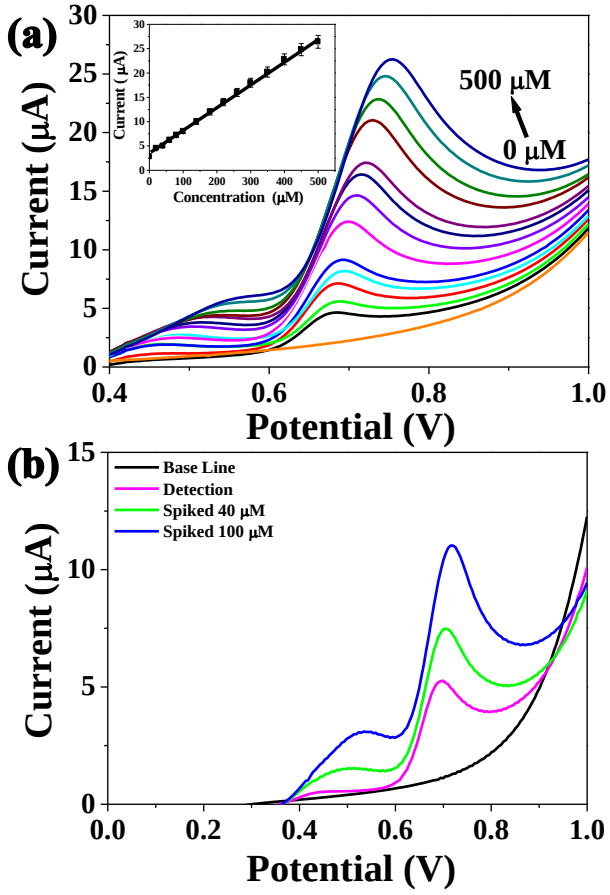

Figure 6 (a) LSVs of $NiCo_2O_4$ modified electrode in the presence of different concentrations of eugenol in 0.1 M citrate buffer (pH 6.0) at a scan rate of 20 mV/s. Inset shows the calibration plot. (b) LSV results of analysis of real sample (Medicative balm sample) using $NiCo_2O_4$ modified electrode in 0.1 M citrate buffer (pH 6.0) at a scan rate of 20 mV/s.

To test the reproducibility of the modified electrode seven $NiCo_2O_4$ modified electrode were prepared by the same way and 50 μM eugenol solutions were determined. As a result, the relative standard deviation (RSD) of ΔI was 5.3% (n = 7). This indicates that the electrode had good reproducibility. In addition, a 50 μM eugenol solution was determined successively for ten times with a $NiCo_2O_4$ modified electrode, and the RSD were found to be 4.8%, which reflected the good repeatability. The storage stability of the electrode was also examined. The electrode was stored at room temperature when not in use and reactivated by dipping in supporting electrolyte for 30 minutes before sensitivity measurement. It was found that after stored in air for 1 week the electrode retained 95.6 % of its initial current response. After stored for 1 month the current response decreased by 7%.

3.5. Analytical application

The ultimate goal of this study is to develop a method with high sensitivity and good selectivity for the detection of eugenol in real samples. The proposed strategy was used for the determination of eugenol in medicative balm samples (Fig. 6(b)). The medicative balm samples were obtained from the local market in Nanyang city. Since the voltammogram has a much sharp and intense peak, target peak can be easily distinguished from any interference, which would be advantageous in real sample analysis (Fig. 6(b)). The concentration of eugenol is calculated according to the calibration curve obtained above. Finally, the standard addition methodology was used to determine the average recovery of eugenol as well as to validate the proposed method. The recoveries of the proposed method are listed in Table S-2 in the ESM. The value of recovery is in the range from 98.7 to 105.5%, also indicating that this method is accurate and feasible. Each sample solution undergoes three parallel detections, and the RSD is below 2%, suggesting that the results obtained by $NiCo_2O_4$ modified electrode are acceptable. Predicated on the results above, we can conjecture that it is possible to fabricate a sensitive electrochemical sensor utilizing $NiCo_2O_4$ modified electrode for the qualitative as well as quantitative detection of eugenol in real samples.

4. Conclusions

In this work, we have demonstrated that $NiCo_2O_4$ nanosheets can be synthesized with sheaf-like

nanostructure morphologies under facile hydrothermal and thermal decomposition process. Further, we demonstrate the usability of a $NiCo_2O_4$ as an electrocatalyst for the electrochemical oxidation of eugenol. The effects of the various experimental conditions on the sensor response and performance were investigated in detail. $NiCo_2O_4$ modified electrode allows a detection concentration of eugenol as low as 5.4 pM. $NiCo_2O_4$ modified electrode has been successfully applied for the detection of eugenol in medicative balm samples. The ease of performance, and good results obtained in terms of recovery in real samples prove the potentiality of this sensor.

Acknowledgements

This work was supported by MOE Tier 1 Grants (RGT8/13 and RG13/13) of Singapore. Authors thank the Facility for Analysis, Characterisation, Testing and Simulation (FACTS) in Nanyang Technological University for materials characterizations.

Electronic Supplementary Material: Supplementary material (XRD pattern of NCHC, Influence of pH on the peak current of eugenol, LSVs at bare glassy carbon electrode, Table S-1 Comparison of analytical performance of $NiCo_2O_4$ modified electrode with sensors reported, Table S-2 Determination of eugenol in real samples) is available in the online version of this article at http://dx.doi.org/10.1007/s12274-***-****-*

References

[1] Son, K. H.; Kwon, S. Y.; Kim, H. P.; Chang, H. W.; Kang, S. S. Constituents from syzygiumaromaticum Merret Perry. *Nat. Prod. Sci.* **1998**, *4*, 263–267.

[2] Wang, H. -F.; Wang, Y. -K.; Yih, K. -H. DPPH free-radical scavenging ability, total phenolic content, and chemical composition analysis of forty-five kinds of essential oils. *J. Cosmet. Sci.* **2008,** *59*, 509–522.

[3] Backheet, E. Y. Micro determination of eugenol, thymol and vanillin in volatile oils and plants. *Phytochem. Anal.* **1998**, *9*, 134–140.

[4] Nam, H.; Kim, M. -M. Eugenol with antioxidant activity inhibits MMP-9 related to metastasis in human fibrosarcoma cells. *Food Chem. Toxicol.* **2013**, *55*, 106–112.

[5] Southwell, I. A.; Russell, M. F.; Davies, N. W. *Flavour Fragrance J.* **2011**, *26*, 336–340.

[6] Sowjanya, J.; Sandhya, T.; Veeresh, B. Ameliorating effect of eugenol on L-arginine induced acute pancreatitis and associated pulmonary complications in rats. *Pharmacologia*. **2012**, *3*, 657–664.

[7] Gülcin, I. Antioxidant activity of eugenol: A structure–activity relationship study. *J. Med. Food* **2011**, *14*, 975–985.

[8] Chang, W. -C.; Hsiao, M. -W.; Wu, H. -C.; Chang, Y. -Y.; Hung, Y. -C.; Ye, J. -C. The analysis of eugenol from the essential oil of Eugenia caryophyllata by HPLC and against the proliferation of cervical cancer cells. *J. Med. Plants Res.* **2011**, *5*, 1121–1127.

[9] Gopu, C. L.; Aher, S.; Mehta, H.; Paradkar, A. R.; Mahadik, K. R. Simultaneous determination of cinnamaldehyde, eugenol and piperine by HPTLC densitometric method. *Phytochem. Anal.* **2008**, *19*, 116–121.

[10] Anu Prathap, M. U.; Sun, S.; Wei. C.; Xu, Z. J. A novel non-enzymatic lindane sensor based on CuO–MnO_2 hierarchical nano-microstructures for enhanced sensitivity. *Chem. Commun.* **2015**, *51*, 4376–4379.

[11] Anu Prathap, M. U.; Srivastava, R. Tailoring properties of polyaniline for simultaneous determination of a quaternary mixture of ascorbic acid, dopamine, uric acid, and tryptophan. *Sens. Actuators, B* **2013**, *177*, 239-250.

[12] Ziyatdinova, G.; Ziganshina, E.; Budnikov, H. Voltammetric sensing and quantification of eugenol using nonionic surfactant self-organized media. *Anal. Methods.* **2013**, *5*, 4750–4756.

[13] Anu Prathap, M. U.; Anuraj, V.; Satpati, B.; Srivastava, R. Facile preparation of $Ni(OH)_2$–MnO_2 hybrid material and its application in the electrocatalytic oxidation of

hydrazine. *J. Hazard. Mater.* **2013**, *262*, 766–774.

[14] Anu Prathap, M. U.; Chaurasia, A. K.; Sawant, S. N.; Apte, S. K. Polyaniline-based highly sensitive microbial biosensor for selective detection of lindane. *Anal. Chem.* **2012**, *84*, 6672–6678.

[15] Anu Prathap, M. U.; Kaur, B; Srivastava, R. Direct synthesis of metal oxide incorporated mesoporous SBA-15 and their applications in non-enzymatic sensing of glucose. *Journal of colloid and interface science* **2013**, *381*, 143-151.

[16] Anu Prathap, M. U.; Satpati, B.; Srivastava, R. Facile preparation of polyaniline/MnO_2 nanofibers and its electrochemical application in the simultaneous determination of catechol, hydroquinone, and resorcinol. *Sens. Actuators, B* **2013**, *186*, 67–77.

[17] Anu Prathap, M. U.; Satpati, B.; Srivastava, R. Facile preparation of β-$Ni(OH)_2$-$NiCo_2O_4$ hybrid nanostructure and its application in the electrocatalytic oxidation of methanol. *Electrochim. Acta* **2014**, *130*, 368–380.

[18] Anu Prathap, M. U.; Srivastava, R. Synthesis of $NiCo_2O_4$ and its application in the electrocatalytic oxidation of methanol. *Nano Energy* **2013**, *2*, 1046–1053.

[19] AnuPrathap, M. U.; Srivastava, R. Electrochemical reduction of lindane (γ-HCH) at $NiCo_2O_4$ modified electrode. *Electrochim. Acta* **2013**, *108*, 145–152.

[20] Wang, Q.; Liu, B.; Wang, X.; Ran, S.; Wang, L.; Chen, D.; Shen, G. Morphology evolution of urchin-like $NiCo_2O_4$ nanostructures and their applications as psuedocapacitors and photoelectrochemical cells. *J. Mater. Chem.* **2012**, *22*, 21647–21653.

[21] Wang, Q.; Wang, X.; Liu, B.; Yu, G.; Hou, X.; Chen, D.; Shen, G. $NiCo_2O_4$ nanowire arrays supported on Ni foam for high-performance flexible all-solid-state supercapacitors. *J. Mater. Chem. A.* **2013**, *1*, 2468–2473.

[22] Wang, Q.; Wang, X.; Xu, J.; Ouyang, X.; Hou, X.; Chen, D.; Wang, R.; Shen, G. Flexible coaxial-type fiber supercapacitor based on $NiCo_2O_4$ nanosheets electrodes. *Nano Energy* 2014, *8*, 44–51.

[23] Mondal, A. K.; Su, D.; Chen, S.; Kretschmer, K.; Xie, X.; Ahn, H. -J., Wang, G. A Microwave synthesis of mesoporous $NiCo_2O_4$ nanosheets as electrode materials for lithium-ion batteries and supercapacitors. *ChemPhysChem* **2015**, *16*, 169–175.

[24] Sun, B.; Zhang, J.; Munroe, P.; Ahn, H. -J.; Wang, G. Hierarchical $NiCo_2O_4$ nanorods as an efficient cathode catalyst for rechargeable non-aqueous Li–O_2 batteries. *Electrochemistry Communications* **2013**, *31*, 88–91.

[25] Mondal, A.K.; Su, D.; Chen, S.; Xie, X.; Wang, G. Highly porous $NiCo_2O_4$ nanoflakes and nanobelts as anode materials for lithium-ion batteries with excellent rate capability, *ACS Appl. Mater. Interfaces* **2014**, *6*, 14827−14835.

[26] Cui, B.; Lin, H.; Li, J. B.; Li, X.; Yang. J.; Tao, J. Core–ring structured $NiCo_2O_4$ nanoplatelets: Synthesis, characterization, and electrocatalytic applications. *Adv. Funct. Mater.* **2008**, *18*, 1440–1447.

[27] Sun, S.; Xu, Z. J. Composition dependence of methanol oxidation activity in nickel-cobalt hydroxides and oxides: an optimization toward highly active electrodes, *Electrochim.Acta* http://dx.doi.org/10.1016/j.electacta.2015.03.008

[28] Li, Q.; Zeng, L.; Wang, J.; Tang, D.; Liu, B.; Chen, G.; Wei, M. Magnetic mesoporous organic−inorganic $NiCo_2O_4$ hybrid nanomaterials for electrochemical immunosensors. *ACS Appl. Mater. Interfaces*. **2011**, *3*, 1366–1373.

[29] Park, K. H.; Jang, K.; Son, S. U. Synthesis, optical properties, and self-Assembly of ultrathin hexagonal In_2S_3 nanoplates. *Angew. Chem., Int. Ed.* **2006**, *45*, 4608–4612.

[30] Tang, J.; Alivisatos, A. P. Crystal splitting in the growth of Bi_2S_3. *Nano. Lett.* **2006**, *6*, 2701–2706.

[31] Xiao, J.; Yang, S. Sequential crystallization of sea urchin-like bimetallic (Ni, Co) carbonate hydroxide and its morphology conserved conversion to porous $NiCo_2O_4$ spinel for pseudocapacitors. *RSC Adv.* **2011**, *1*, 588–595.

[32] Fan, Z.; Chen, J.; Cui, K.; Sun, F.; Xu, Y.; Kuang, Y. Preparation and capacitive properties of cobalt–nickel oxides/carbon nanotube composites. *Electrochim. Acta* **2007**, *52*, 2959–2965.

[33] Wei, T. Y.; Chen, C. H.; Chien, H. C.; Lu, S. Y.; Hu, C. C. A cost-effective supercapacitor material of ultrahigh specific capacitances: spinel nickel cobaltite aerogels from an epoxide-driven sol–gel process. *Adv. Mater.* **2010**, *22*, 347–351.

[34] Nie, H.; Yao, Z.; Zhou, X.; Yang, Z.; Huang, S. Nonenzymatic electrochemical detection of glucose using well-distributed nickel nanoparticles on straight multi-walled carbon nanotubes. *Biosens. Bioelectron.* **2011**, *30*, 28–34.

[35] Mocak, J.; Bond, A. M.; Mitchell, S.; Scollary, G. A statistical overview of standard (IUPAC and ACS) and new procedures for determining the limits of detection and quantification: application to voltammetric and stripping techniques. *Pure Appl. Chem.* **1997**, *69*, 297–328.

[36] Yu, B. -S.; Lai, S. -G.; Tan Q. -L. Simultaneous determination of cinnamaldehyde, eugenol and paeonol in traditional chinese medicinal preparations by capillary GC-FID. *Chem. Pharm. Bull.* **2005**, *54*, 114–116.

[37] Saran, S.; Menon, S.; Shailajan, S.; Pokharna, P. Validated RP-HPLC method to estimate eugenol from commercial formulations like caturjata churna, lavangadi vati, jatiphaladi churna, sitopaladi churna and clove oil. *J. Pharm. Res.* **2013**, *6*, 53–60.

[38] Luque, M.; Ríos, A.; Valcárcel, M. Use of supported liquid membranes incorporated in a flow system for the direct determination of eugenol in spice samples. *The Analyst* **2000**, *125*, 1805–1809.

[39] Feng, Q.; Duan, K.; Ye, X.; Lu, D.; Du, Y.; Wang, C. A novel way for detection of eugenol via poly (diallyldimethylammonium chloride) functionalized graphene-MoS_2 nano-flower fabricated electrochemical sensor. *Sens. Actuators, B* **2014**, *192*, 1– 8.

[40] Kang, S. -Z.; Liu, H.; Li, X.; Sun. M.; Mu, J. Electrochemical behavior of eugenol on TiO_2 nanotubes improved with Cu_2O clusters. *RSC Adv.* **2014**, *4*, 538–543.

[41] Afzali, D.; Zarei, S.; Fathirad, F.; Mostafavi, A. Gold nanoparticles modified carbon paste electrode for differential pulse voltammetric determination of eugenol. *Mater. Sci. Eng. C* **2014**, *43*, 97–101.

[42] Huang, J.; Liu, Y.; Hou, H.; You, T. Simultaneous electrochemical determination of dopamine, uric acid and ascorbic acid using palladium nanoparticle-loaded carbon nanofibers modified electrode. *Biosens. Bioelectron.* **2008**, *24*, 632–637.

Electronic Supplementary Material

A New Insight into Electrochemical Detection of Eugenol by Hierarchical Sheaf-like Mesoporous $NiCo_2O_4$

M.U. Anu Prathap, Chao Wei, Shengnan Sun and Zhichuan J. Xu(✉)

School of Materials Science and Engineering, Nanyang Technological University, 50 Nanyang Avenue, Singapore 639798, Singapore

Supporting information to DOI 10.1007/s12274-****-****-* (automatically inserted by the publisher)

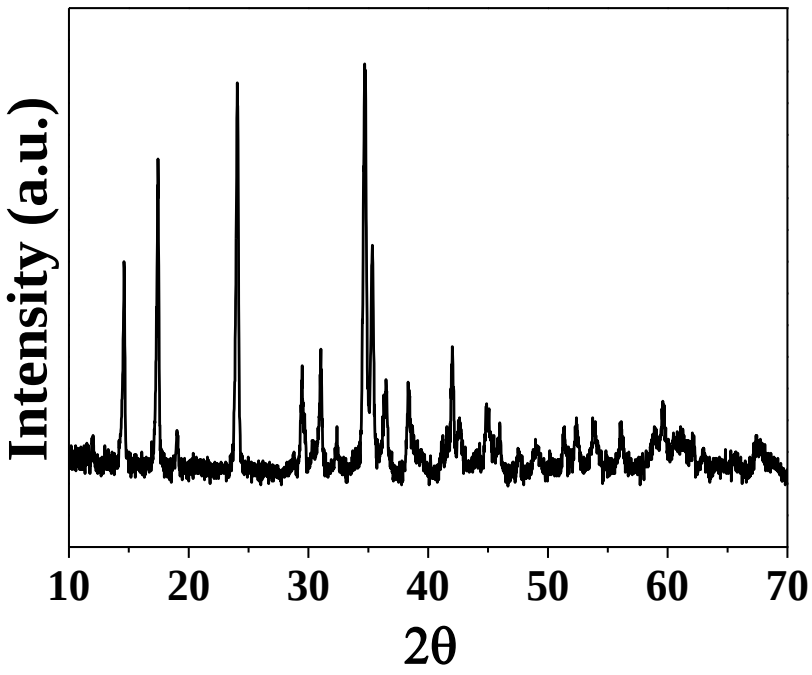

Figure S-1 XRD pattern of nickel cobalt hydroxy carbonate.

Address correspondence to xuzc@ntu.edu.sg

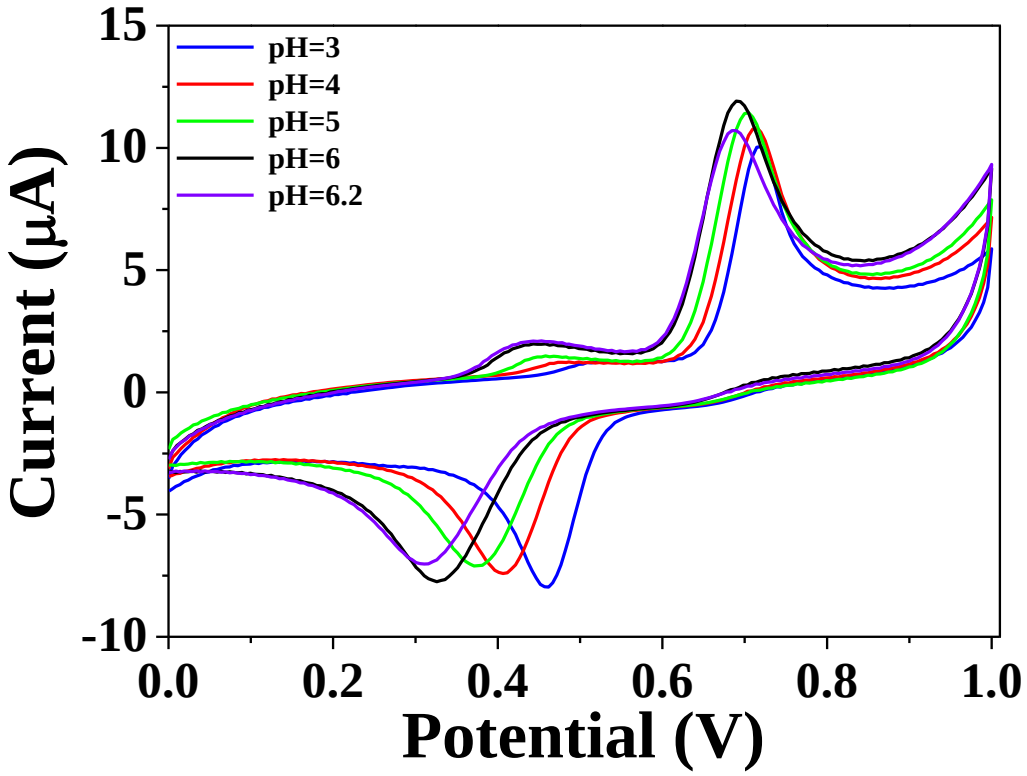

Figure S-2 Influence of pH on the peak current of eugenol. Scan rate = 20 mV/s.

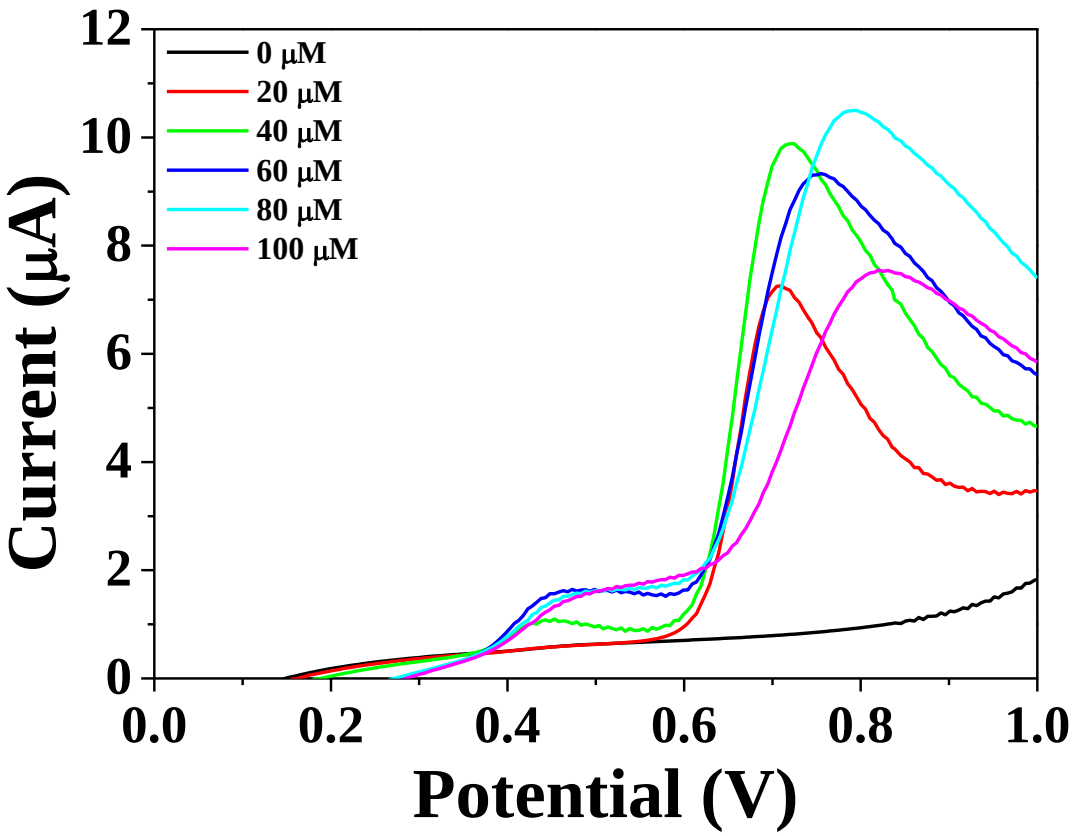

Figure S-3 LSVs at bare glassy carbon electrode in the presence of different concentrations of eugenol in 0.1 M citrate buffer solutions at a scan rate of 20 mV/s. Inset shows the calibration plot.

Table S-1 Comparison of analytical performance of $NiCo_2O_4$ modified electrode with sensors reported for electrocatalytic detection of eugenol.

	Linear range	**Detection limit**	**References**
Method			
GC-FID	1.89–3806 μM	1.2 μM	[30]
RP-HPLC	0.30–304.5 μM	0.15 μM	[31]
Electrode			
PVC-graphite/electrode	3.04–182.7 μM	1.01 μM	[32]
Au/PDDA-G-MoS_2/GCE	0.1–440 μM	0.036 μM	[33]
Triton X100/Brij 35/GCE	15–1230 μM	3.8 μM	[12]
TiO_2-Cu_2O clusters	4.6–460 μM	1.3 μM	[34]
Gold nanoparticle/CPE	5–250 μM	2.0 μM	[35]
$NiCo_2O_4$	1 μM–500 μM	5.4 pM	Present study

GC-FID = Gas chromatography-Flame ionization detector; **RP-HPLC** = Reversed phase-High performance liquid chromatography; **PVC** = Polyvinyl chloride; **PDDA-G** = Poly diallyl dimethyl ammonium chloride-graphene**; GCE** = Glassy carbon electrode; **CPE** = Carbon paste electrode; **pM =** Picomolar

Table S-2 Determination of eugenol in real samples.

Sample	Measured (μM)	Added (μM)	Found (μM)	RSD (%)	Recovery (%)
#1[a]	60	40	101.3 ± 0.01	1	102.1[b]
		100	163.3 ± 0.01	1.8	105.5
#2	75	10	86.3 ± 0.01	1.3	101.7
		100	174 ± 0.01	0.79	98.7

[a] Samples: #1 and #2: Medicative balm samples; all purchased from a super market in Nanyang city.
[b] % Recovery = 100 × (c_{Found}-cspiked/c).